POWER CONTROL STRATEGY FOR GRID-CONNECTED INVERTERS IN STATIONARY REFERENCE FRAME

Lucas S. Xavier[1], Allan F. Cupertino[2], Heverton A. Pereira[3], Victor F. Mendes[1]
[1]Graduate Program in Electrical Engineering - Universidade Federal de Minas Gerais - Belo Horizonte, MG, Brazil
[2]Department of Materials Engineering, Federal Center for Technological Education of Minas Gerais - Belo Horizonte, MG, Brazil
[3]Department of Electrical Engineering, Universidade Federal de Viçosa - Viçosa, MG, Brazil
e-mail: lsx@ufmg.br, afcupertino@ieee.org, heverton.pereira@ufv.br, victormendes@cpdee.ufmg.br

***Abstract* – The control of grid-connected converters in stationary reference frame has been investigated in several works of literature. One of the challenges of this method is in the computation of the current computing current references as a function of power references. In some works, this issue has been solved based on instantaneous power theory equations described in the stationary reference frame. However, this approach can lead to steady-state errors in the injected power if there is an error in the current control loop, which is the focus of this investigation. Firstly, analytical expressions are derived to investigate the effect of current loop steady-state error in the active and reactive power injected into the grid. Then, this paper proposes a closed-loop power control for grid-connected inverters controlled in the stationary reference frame. This strategy is experimentally investigated in two power conversion system configurations for battery energy storage systems. The results indicate that the proposed scheme guarantees zero steady-state error in the injected power even when the current loop presents an amplitude and phase steady-state error.**

***Keywords* – Active Power Control, Battery Energy Storage Systems, Instantaneous Power Theory, Reactive Power Control, Square Voltage Control, Stationary Reference Frame**

I. INTRODUCTION

The cost reduction of battery technologies and high penetration level of photovoltaic and wind energy generation in the electrical power systems contribute to the growth of battery energy storage systems (BESS) installations around the world [1]. Furthermore, the BESS can contribute to several grid services, which increases the hosting capacity of distributed generation (DG) [2]. The main services are time-shifting (arbitrage), peak shaving, load leveling, spinning reserve, voltage support, support of intermittent renewable generation plants and reactive power support [3].

All these services involve the control of active or reactive power in the grid. Generally, the reactive power is controlled in the outer-loop of the inverter control strategy, which composes the dc/ac stage of the power conversion system (PCS). The inner-loop, responsible for controlling the inverter current, can be implemented in different reference frames, such as synchronous rotating (dq), stationary ($\alpha\beta$) and (abc) reference frames [4]. Reference [5] concludes that synchronous reference frames are most sensitive to voltage distortions and unbalances in the point of common coupling (PCC).

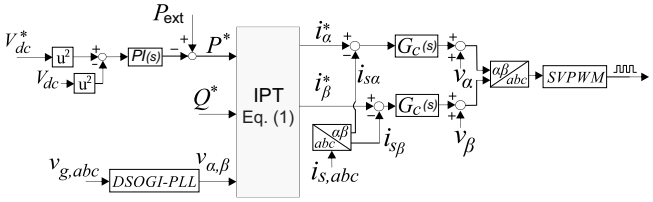

Fig. 1. Inverter control strategy based on square dc-link along with the stationary reference frame and IPT.

Generally, the inverter controls the active power indirectly through the dc-link voltage control. The literature presents two main approaches to controlling the dc-link voltage. The first one is controlling directly the measured value [6]. The second approach is controlling through the square value of the measurement [7]. Generally, the square voltage-based method is associated with the instantaneous power theory (IPT) to calculate the inverter reference current in the stationary reference frame. The advantage of using the square dc-link voltage-based method along with the stationary reference frame and IPT, shown in Figure 1, are listed below [8]:

- This control strategy presents a normalization by grid voltage amplitude, improving the dynamic of the dc-link voltage during sags;
- This strategy does not require Park transformation;
- Less sensitive to voltage distortions and unbalances in the PCC;
- This strategy presents active power reference explicitly, which is helpful for current dynamic saturation.

However, generally, this control strategy is used with reactive power in an open loop, as shown in Figure 1 [9]. This approach leads to a steady-state error in reactive power component if the current control presents any errors. For this reason, reference [8] proposes a control strategy in a closed-loop for reactive power. However, experimental validation is required. Furthermore, there are cases where the active power must be controlled directly by the inverter control. Generally, this approach is adopted when the dc/dc converters of the PCS are cascaded connected. This PCS structure has been gaining attention for BESS application due to the low

Manuscript received 11/27/2021; first revision 03/16/2022; accepted for publication 07/25/2022, by recommendation of Editor Marcelo Lobo Heldwein. http://dx.doi.org/10.18618/REP.2022.2.0048

step-up ratio if compared to the parallel converter structure [10]. In this case, the dc-link voltage is controlled by dc/dc converters, and the inverter directly controls the active and reactive power exchanged with the grid. Therefore, a closed-loop control strategy is also required for the active power component control.

Given the above discussions, the main contributions of this paper are listed below:

- Mathematical analysis of the error in the power components if the open loops are used;
- Proposal of a closed-loop for active power applied in the control strategy based on stationary reference frame and IPT;
- Experimental validation of reactive power closed-loop applied in dc-link voltage-based method along with stationary reference frame and IPT.

It is worth noting that the proposal of this work apply to any system that presents grid-connected inverters, such as photovoltaic, wind, and battery energy storage systems. In this work, proposed control strategies are studied and applied in battery energy storage systems due to their current importance for distributed generation.

This paper is organized into six sections. Section II presents the power structure where the control strategies are studied and validated. In Section III, the control strategies proposed in this work are detailed. Section IV shows the control design of the proposed control strategies. The error modeling on the active and reactive power is performed in Section V. Experimental results are presented in section VI. Finally, the conclusions are presented in section VII.

II. POWER ELECTRONICS STRUCTURES FOR BESS REALIZATION

The proposed reactive and active power control strategies based on stationary reference-frame and instantaneous power theory are applied and analyzed in the control structures shown in Figure 2. These structures are grid-connected BESS, which present PCS of two stages. The first stage is composed by the inverter and the second stage is composed by dc/dc converters.

In the first stage, a two-level inverter is used to interface the BESS system with the grid. In the second stage, a multiport power electronic concept is used in [11]. With this approach, it is possible to associate different sources and battery technologies and operate in different power levels, improving power management and flexibility.

This work uses two approaches to multiport converters with interleaved bidirectional dc/dc converters, which is interesting to reduce the input and output current ripple [12], [13]. In this work, three legs are used for each dc/dc converter.

The first analyzed multiport converter structure uses two interleaved bidirectional dc/dc converters connected in parallel, as shown in Figure 2.a. The association of dc/dc converters in parallel mode is widely discussed in literature [14]–[16]. The voltage outputs of the dc/dc converters are equal to the dc-link voltage, which is generally regulated by the inverter control scheme. In this scenario, each dc/dc converter can inject power independently and the typical outer-

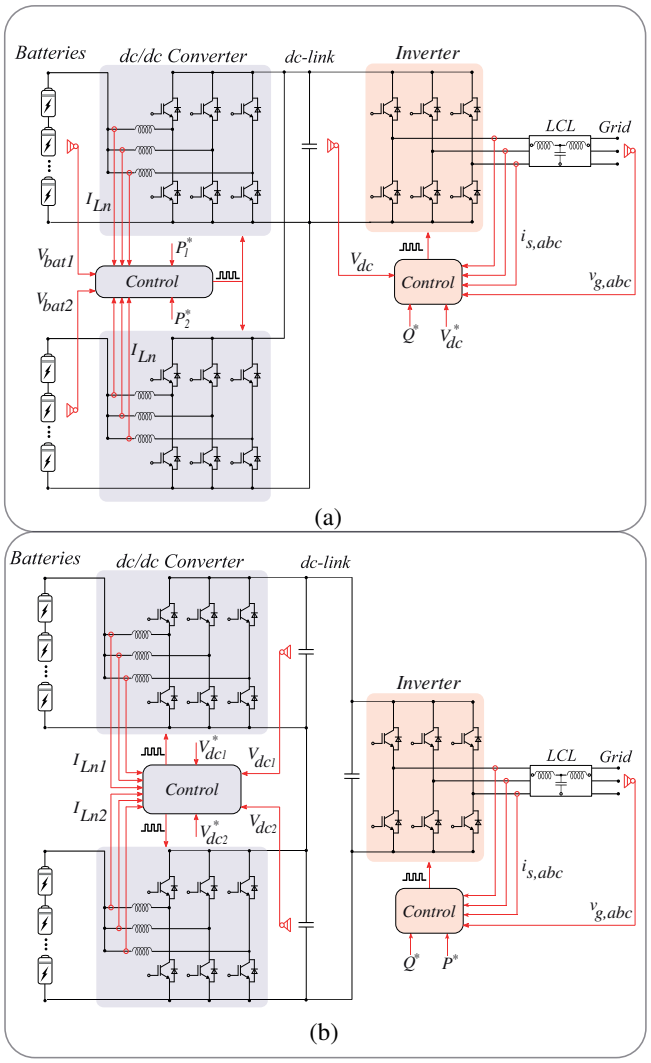

Fig. 2. Power structures based on grid-connected BESS composed of PCS two stages. (a) Parallel connection of two interleaved dc/dc converters. (b) Cascaded connection of two interleaved dc/dc converters.

loop of the control strategy have the following characteristics:

- The inverter control strategy presents the dc-link voltage (V_{dc}) and reactive power (Q) control. The control references for both quantities are V_{dc}^* and Q^*, respectively.
- The dc/dc converters control the active power (P_1) and (P_2) processed by each one independently, according to the references are (P_1^*) and (P_2^*).

An advantage of the parallel connection lies in the fact that if one converter fails, it can be removed from the system effortlessly due to the natural independence connection between the converters With penalties on power rating. A disadvantage is the high voltage step-up ratio required for a low input voltage, reducing the efficiency.

The second multiport dc/dc converters is the cascaded connection of two interleaved bidirectional dc/dc converters, as shown in Figure 2.b [10], [17], [18]. The advantage of this structure is the sum of the output voltage of the converters, allowing the lower voltage step-up ratio required if compared

to the parallel structure [19]. However, there are challenges in the control and power structure of this strategy. This structure requires an equal output current in each dc/dc converter. Therefore, bypass diodes are required for this structure to remove a converter in case of failure [10]. For simplicity, these diodes are not shown in Figure 2.b.

Furthermore, the output voltage of each converter cannot be fixed by the inverter control, as performed in the parallel structure. Therefore, each dc/dc converter controls its output voltage and the power control is transferred for the inverter control strategy. In this scenario, the independent operation between the dc/dc converters is achieved by changing their output voltages [19]. Therefore, if the dc-link is kept constant, the output voltages of the dc/dc converter must be changing proportionally to the power operation point in each one. For this structure, the typical outer loop of the control strategy has the following characteristics:

- The inverter control strategy have the active (P) and reactive power (Q) control;
- The dc/dc converters control the output dc voltage (V_{dc1}) and (V_{dc2}), which follows the references (V^*_{dc1}) and (V^*_{dc2}).

It is important to highlight that inner loops of both structures are similar, and they are responsible for controlling the inverter output current and current of each arm of the interleaved dc/dc converter. However, the focus of this work is on the outer loop of the inverter control strategy and this discussion is deepened in the next section.

III. CONTROL STRUCTURES

The typical inverter control structure discussed in literature are based on the dc-link voltage square V_{dc} in outer-loop and stationary reference-frame, the current control is shown in Figure 3.a [9], [20], [21]. This control strategy can integrate the inverter control structure shown in Figure 2.a, since this is responsible for dc-link voltage control.

The modeling of the outer-loop based on the V_{dc} squared method is carried out from the stored energy in the dc-link capacitor, detailed in [22]. A proportional-integrator (PI) controller calculates the power which is required in the dc-link capacitor bank to regulate the dc-link voltage to the reference V^*_{dc}. Therefore, through the external power P_{ext} measured in the battery bank terminals, the inverter active power reference (P^*) is calculated.

The inverter current references ($i^*_{\alpha,\beta}$) in the stationary reference frame are calculated by the instantaneous power theory, given by [23]:

$$\begin{bmatrix} i^*_\alpha \\ i^*_\beta \end{bmatrix} = \frac{1}{v_\alpha^2 + v_\beta^2} \begin{bmatrix} v_\alpha & v_\beta \\ v_\beta & -v_\alpha \end{bmatrix} \begin{bmatrix} P^* \\ Q^* \end{bmatrix}, \tag{1}$$

where Q^* is the reactive power reference to perform some grid service such as Low-Voltage-Ride-Through, or voltage regulation [24], [25]. The positive sequence on the fundamental frequency of the point of common coupling (PCC) voltage in stationary reference ($v_{\alpha,\beta}$) is calculated by the dual second-order generalized integrator (DSOGI) with the

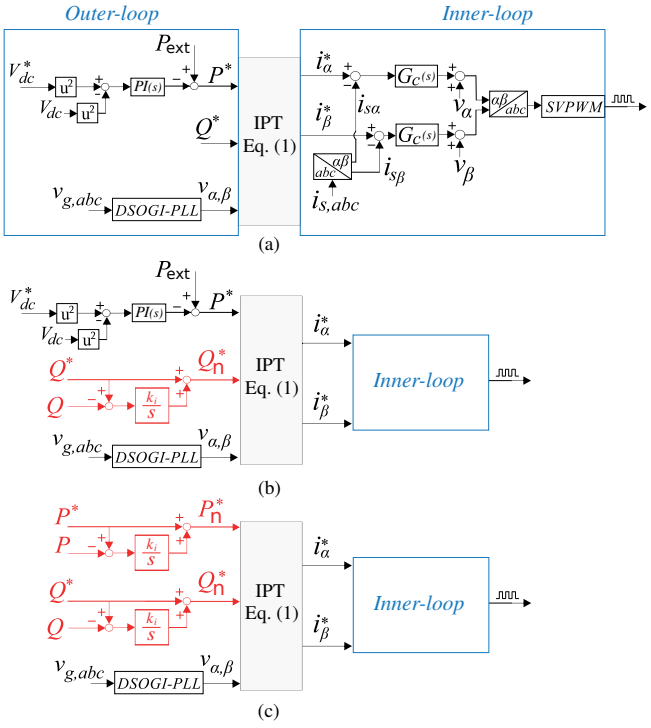

Fig. 3. Inverter control structure approached in this work. (a) Traditional control structure based on V_{dc} square method and stationary reference frame. (b) Modified control structure with reactive power closed loop. (c) Proposed active power closed loop for the approached control strategy.

phase-locked loop (PLL). Reference [26] presents a complete description of this structure.

The inner-loop present the current controller G_c to control the inverter current in the stationary reference-frame. In this work, the proportional-resonant (PR) controller is used which the transfer function given by [27]:

$$G_c = K_{pi} + K_r \frac{s}{s^2 + \omega^2}, \tag{2}$$

where K_{pi} is the proportional gain, K_r is the resonant gain and ω is the resonant frequency. The PR controller design is described in [28]. Finally, the feedforward voltage terms ($v_{\alpha,\beta}$) are included, generating the inverter reference voltages synthesized using a space vector modulation (SVPWM).

As can be seen, the reactive power is essential in the open-loop in this scheme. This approach presents steady-state error in the reactive injection and leads to poor performance of the reactive services performed by the inverter. For this reason, reference [8] proposes the reactive power control loop for the control structure that uses V_{dc} squared based method for dc-link voltage control and stationary reference-frame in the current control, as shown in Figure 3.b. This control technique adds the measured inverter reactive power (Q) and compares it with the reference (Q^*). An integrator controller (k_i/s) processes the error between these two components and the output is added to the reference Q^*, equaling this reference to the measured component in steady-state. This control strategy is applied in the power structure shown in Figure 2.a, where the inverter controls the dc-link voltage and the parallel dc/dc converters control the system power.

When the cascaded dc/dc converters are employed, as

shown in Figure 2.b, the dc-link voltage control is transferred to the dc/dc converters and the active power is performed by the inverter. This approach allows using the stationary reference frame in the current control with instantaneous power theory and ensures an easy saturation of power components processed by the inverter. Therefore, this work extends the method proposed for the reactive power control to the active power control, as shown in Figure 3.c. In the next section, a control analysis is performed for both the reactive and active power loops.

Active and active power is measured through the voltage and current components of the inverter in the stationary reference frame, given by [29]:

$$P = \frac{1}{2}(v_\alpha i^*_\alpha + v_\beta i^*_\beta) \tag{3}$$

$$Q = \frac{1}{2}(v_\beta i*_\alpha - v_\alpha i*_\beta). \tag{4}$$

IV. ERROR MODELLING ON THE ACTIVE AND REACTIVE POWER

The power components error can be modeled as a function of phase and amplitude errors in current control loops. For this purpose, considering the active (P) and reactive (Q) power components injected by the inverter given by:

$$P = \frac{3}{2}(v_\alpha i_\alpha + v_\beta i_\beta), \tag{5}$$

$$Q = \frac{3}{2}(v_\beta i_\alpha - v_\alpha i_\beta), \tag{6}$$

where $v_{\alpha\beta}$ is the grid voltage in stationary reference frame, $i_{\alpha\beta}$ is the output current of the inverter. These voltage and current components are substituted by:

$$v_\alpha = V\cos(\omega t), \tag{7}$$
$$v_\beta = V\cos(\omega t - 90), \tag{8}$$
$$i_\alpha = (I + \Delta I)\cos(\omega t + \delta + \Delta\theta), \tag{9}$$
$$i_\beta = (I + \Delta I)\cos(\omega t - 90 + \delta + \Delta\theta), \tag{10}$$

where V is the peak value of grid phase voltage, I is the peak value of the inverter current, ΔI is the amplitude error of current controller, $\Delta\theta$ is the current controller phase error and δ is the angle of the power factor (PF) the current controller phase error.

Therefore, errors in active and reactive power are given by, respectively:

$$\Delta P = P^* - P = \frac{3}{2}V[(I + \Delta I)\cos(\delta + \Delta\theta) - I\cos(\delta)], \tag{11}$$

$$\Delta Q = Q^* - Q = \frac{3}{2}V[(I + \Delta I)\sin(\delta + \Delta\theta) - I\sin(\delta)], \tag{12}$$

Considering same current and voltage amplitudes, the errors depend on PF angle, the amplitude and phase error

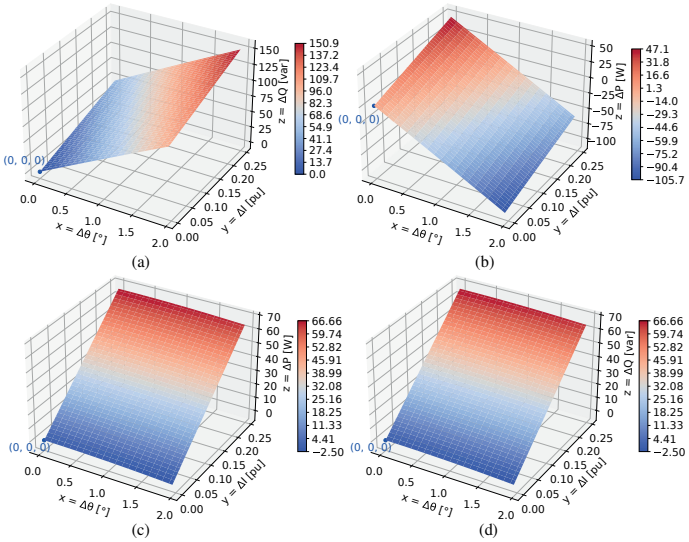

Fig. 4. Active and reactive power error in relation to the phase and amplitude errors of the current control, considering different power factors. (a) Reactive power error for PF = 0.707. (b) Active power error for PF = 0.707. (c) Active power error for PF = 1. (d) Reactive power error for PF close to 0.

of the current control. Power components errors are shown in Figure 4 considering $V = 180\ V$, $I = 16\ A$, regarding the current control errors ($\Delta\theta$ and ΔI). The power factors equal to 0.707, 0 and 1 are used in this analysis. It can be noticed that the PF has a great influence on the error plan shape between the cases. For $PF = 0.707$, the $\Delta\theta$ has the predominant influence on the error in both power components compared with ΔI. For $PF = 1$ and 0, the ΔI has a predominant influence on the error.

This analysis confirms that any current control errors lead to errors in the power components and the closed-loop is important. The current control error can arise due to the frequency grid variation, discretization problems and worse control tunning.

V. DESIGN OF THE POWER CONTROLS

The current reference frame addressed in this work is stationary and thus the current controller must be able to track signal with a specific frequency. In this scenario, the use of a proportional-integral controller leads to magnitude and phase errors [30]. Because of that, the proportional-resonant controllers (PR) have been spread used in this scenario [31].

The active and reactive power errors in steady-state, using the open-loop approaches are mainly due to phase or amplitude error from current control. These errors can occur even if current control strategy is well-tuned. For example, if proportional-resonant (PR) controllers, tunned at 60 Hz, are used, in case of grid voltage and frequency instabilities the active and reactive power error arises. To overcome this drawback, adaptive PR controller tunning can be used [31]. However, this approach requires considerable computational time processing since recommended discretization based on Tustin, with pre-warping, requires the calculation of trigonometric functions in all execution steps [32].

This drawback can be better understood through the bode diagram of the inverter current closed-loop, shown in Figure 5.

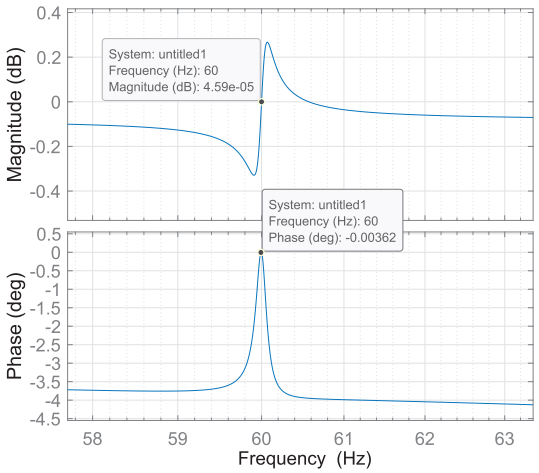

Fig. 5. Bode diagram of the inverter current closed loop. (a) Magnitude. (b) Phase.

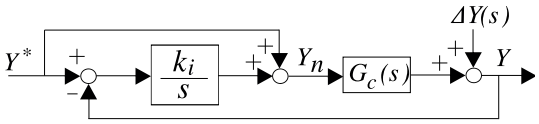

Fig. 6. Simplified closed loop block diagram of the active and reactive power controls.

In this example, the PR controller is designed to track the 60 HZ current, however, there are magnitude and phase errors if the signal frequency changes, for example, to 60.5 Hz.

To overcome this drawback, the second solution is to use the proposed closed-loop strategies for power components control. However, an important step in using this technique is the design of the controllers. can be seen in Figure 3.c, both active and reactive power control loops have a similar structure. Therefore, these control loops have the same design and, consequently, the same stability analysis.

The simplified closed-loop block diagram of the active and reactive power controls is shown in Figure 6, where Y represents both power components and k_i/s is the integral controller. G_c is the inner loop controller, which is designed to be faster than the outer-loop control. In such conditions, $G_c \approx 1$. $\Delta Y(s)$ is the disturbance that causes steady-state error in the power components concerning the references. The output dynamic stiffness, which indicates the effect of the disturbance $\Delta Y(s)$ in the output power component Y, can be found as:

$$\frac{\Delta Y(s)}{Y(s)} = 1 + \frac{k_i}{s}, \tag{13}$$

where k_i is the integrator gain. This relationship describes the effect of the disturbance in the output $Y(s)$. Figure 7 shows the dynamic stiffness magnitude concerning the frequency for range values of k_i. It is important to note that $k_i = 0$ represents the case when the power components are in an open loop, presenting a poor dynamic stiffness. In this case, a unitary magnitude of ΔY causes a unitary magnitude error in the output Y in all frequency spectrums. As k_i increases, the dynamic stiffness increases for $s \to 0$ and still is unitary for $s \to \infty$. Therefore, theoretically, the higher the value of k_i, the better the dynamic stiffness.

Ignoring the constant term Y^* adding to the output of

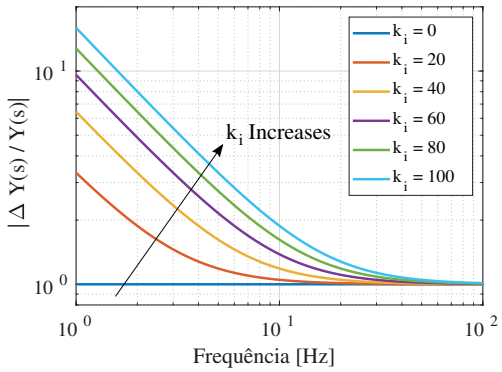

Fig. 7. Dynamic stiffness of the power loops in relation to the integrator gain k_i.

the controller k_i/s and ΔY, the closed loop transfer function reported in Figure 6 is given by:

$$\frac{Y^*(s)}{Y(s)} = \frac{k_i}{s + k_i}, \tag{14}$$

The pole of this transfer function is:

$$\omega_c = k_i, \tag{15}$$

Generally, the inner-loop control is designed one decade below the inverter switching frequency. The pole is placed three decades below the switching frequency, k_i can be estimated by:

$$k_i = \frac{2\pi}{1000 T_{sw}}, \tag{16}$$

where T_{sw} is inverter switching period.

Therefore, the control design of the power components is performed to take into account the maximum dynamics stiffness as possible, respecting the limited frequency response concerning the inner-loop.

VI. RESULTS

A 6 kVA BESS is used in simulation and experimental setup to validate the control strategies of the power components shown in Figure 3. The response of the proposed power control loops during frequency variations is shown in simulation results. Furthermore, a comparison between the proposed methodology and one already present in the literature is shown in the simulation results. In the experimental test bench, steady-state comparisons between the closed-loop of the power components and the open-loop approach are shown. In the simulation results, the topology is shown in Figure 2.b is used. In experimental results, both topologies of Figure 2 are used.

The main parameters of the system for both simulation and experimental test setup are shown in Tab. I. the PR controllers are used in the current control, tuned at the 60 Hz rated frequency of the grid. The inner-loop control frequency of the inverter is designed a decade below the switching frequency. The outer-loop reactive and active power components control are designed three decades below the switching frequency, given k_i equal to 57.

TABLE I
Simulation and Experimental System Parameters

Power Parameters	Value
LCL inductances	1 mH
LCL capacitance	25 μF
Dc-link capacitance	4.7 mF
Interleaved dc/dc Converter inductance	4 mH
Switching frequencies	9 kHz
Grid line Voltage	220 V

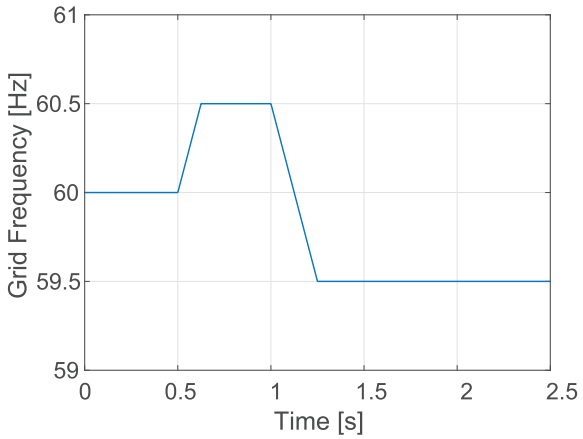

Fig. 8. Grid frequency variation for the simulation case study.

A. Simulation Results

The grid frequency is changed to demonstrate the performance of the proposed power control loops, as shown in Figure 8. The frequency begins at 60 Hz. In 0.5 seconds, it is changed to 60.5 at a slope rate of 4 Hz/second. In 1 second, the frequency changes to 59.5 Hz at the same slop rate.

The time responses of active and reactive power during grid frequency variation is shown in Figures 9.a and 9.b, respectively. It can be noticed the disturbances during the frequency transitions and their rejection in steady-state, according to the controller design. The grid frequency transients occur when the active and reactive power is equal to 3000 W and 3000 var, respectively. Furthermore, there are transients in 1.5 and 2 seconds in both active and reactive power, respectively, dropping to half of the initial conditions. Results show a fast closed-loop response time.

Figure 10 shows the same time responses and transients for a power control strategy present in the literature [33]. This strategy controls the inverter current in the stationary reference frame, likely the proposed strategy in this work. However, it does not use the instantaneous power theory to calculate the reference current, since the response of the outer loop controller is the conductance. For a fair comparison, the outer loop controllers are adjusted to have the same bandwidth and dynamic stiffness as the strategy proposed in this work. It can be verified a similarity between the strategies during the transitions of the grid frequency and also in the power variation, showing the applicability of the proposed strategy near to the existing one.

Finally, Figures 11.a and 11.b show the active and reactive power components considering the open-loop, respectively.

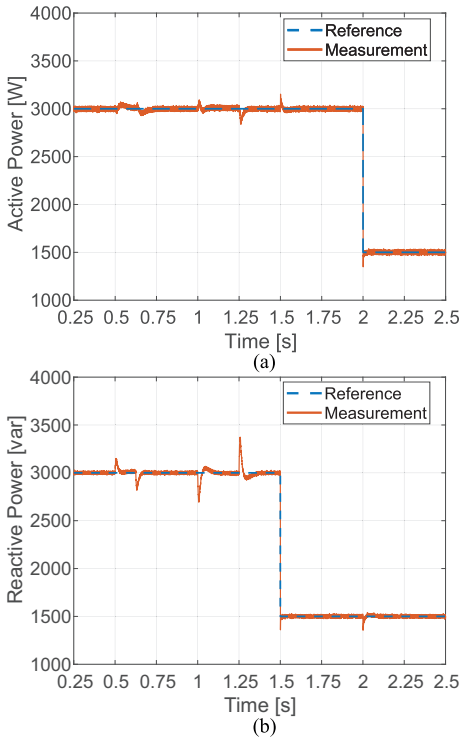

Fig. 9. Reference and measurement of the active and reactive powers with proposed control loops. (a) Active power. (b) Reactive power.

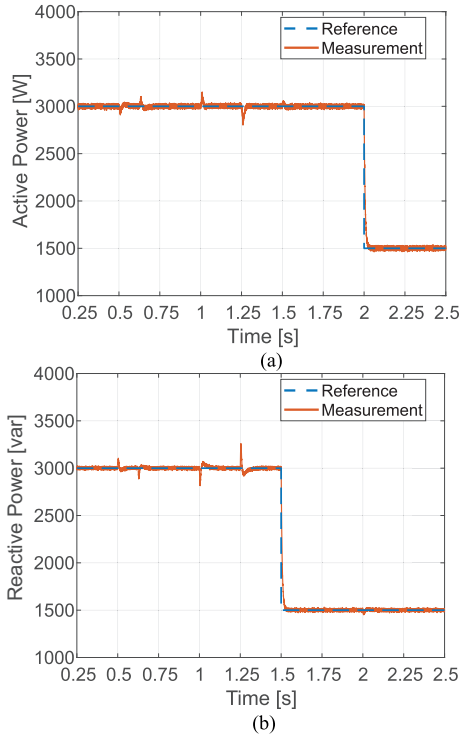

Fig. 10. Reference and measurement of the active and reactive powers with control loops presented in literature. (a) Active power. (b) Reactive power.

Note the steady-state error in the power components with the grid frequency variations.

B. Experimental Results

A 6 kVA experimental BESS bench is used to validate the power components control strategies shown in Figure 3.

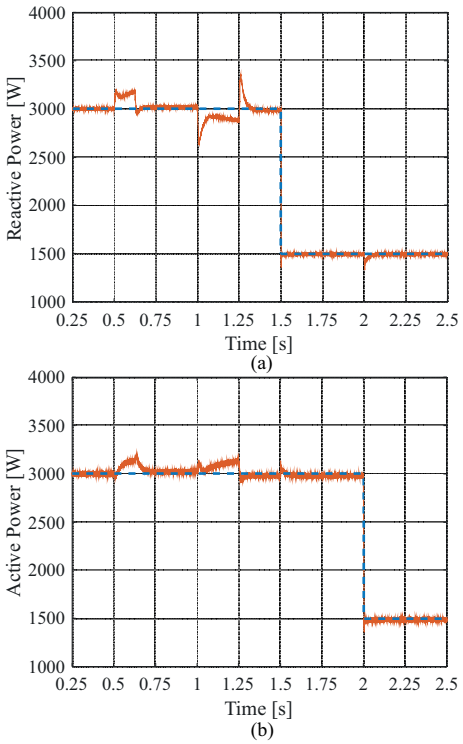

Fig. 11. Reference and measurement of the active and reactive powers using the power components in open-loop. (a) Active power. (b) Reactive power.

This setup allows implementing both parallel connection and cascaded connection of dc/dc converters. The experimental setup overview is shown in Figure 12. The main parameters of the BESS are shown in Tab. I. The control structures are implemented in two TMDSDOCK28379D experimental kits with the DSP F28379D from Texas Instruments.

The rms grid line voltage is 220 V and PR controllers used in the current control, tuned at the 60 Hz grid rated frequency. To demonstrate the errors that can happen in inverter current control, the test bench was supplied with a power source that imposes a frequency of 60.5 Hz. The Regenerative Grid Simulator NHR 9410 is used to perform a frequency variation. This scenario is suitable to validate the control strategies. It is important to highlight that this was the simplest manner of emulating a control error.

Lead-acid batteries 12MN36 of MOURA with a voltage of 12 V and charge of 36 A at 20*C* are used. Each dc/dc converter presents 16 batteries in series. The dc-link voltage is controlled at 480 V during the experiment.

The inner-loop control frequency of the inverter is designed a decade below the switching frequency. The outer-loop reactive and active power components control are designed three decades below the switching frequency, given k_i equal to 57.

The first analysis considers the structure shown in Figure 2.a, with two interleaved dc/dc converters in parallel connection. In this case, the reactive power regulation considering control structure in open and closed loops for reactive power is shown in Figures 3.a and 3.b, respectively. Figure 13 shows reactive power profile considering PF equal to 0.707 and reference equal to 3000 var. It can be noticed that open-loop approach presents an error between measurement

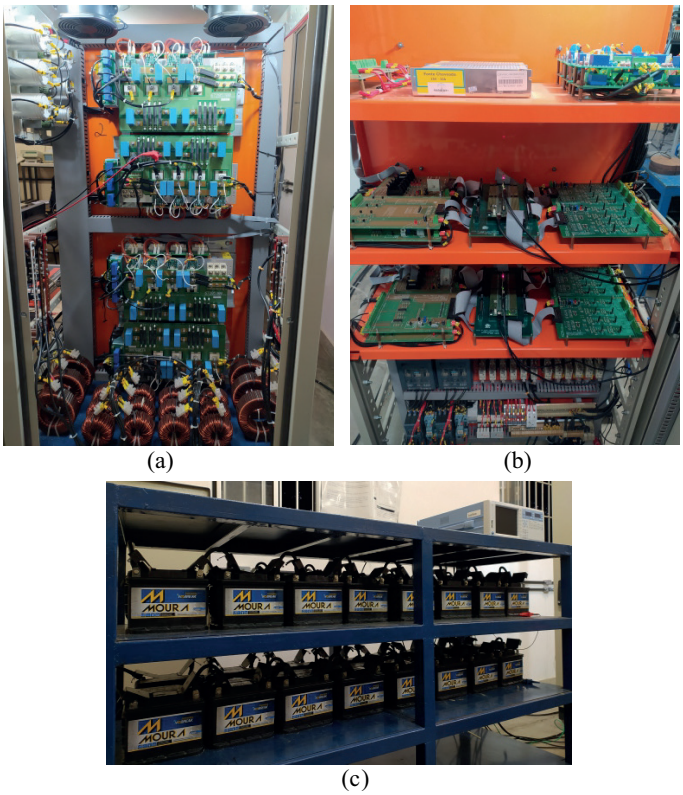

Fig. 12. Experimental bench overview. (a) Power Structure. (b) Control Structure. (c) Lead-acid battery bank.

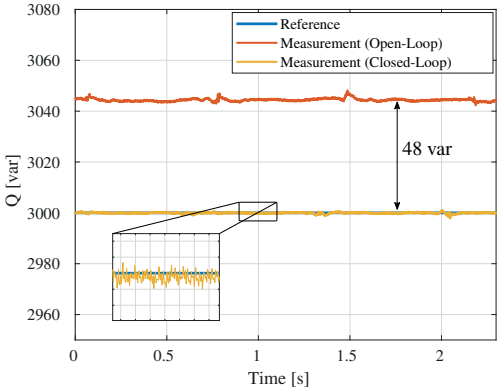

Fig. 13. Reactive power profile considering power structure composed of two interleaved dc/dc converters in parallel connection and power factor equal to 0.707, considering reactive power in open and closed loop with reference equal to 3000 var.

and reference equal to 48 var, while for closed-loop approach, the error of measured reactive power and reference is close to zero.

The reference and measurement current of inverter inner control loop are shown in Figure 14, considering the reactive power open-loop approach. The phase error ($\Delta\theta$) between these two components is 0.84 degrees and the amplitude error (ΔI) is 0.03 pu. These errors were estimated through the Fast Fourier transform. Through the mathematical analysis presented in previous section, the expected reactive power error is 50.25 var. This represents an estimation error of 4.7% concerning the measurement value of 48 var, as shown in Figure 13.

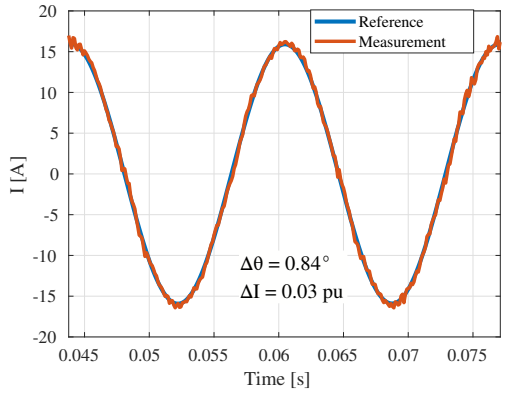

Fig. 14. Reference and measurement current of inverter inner control loop.

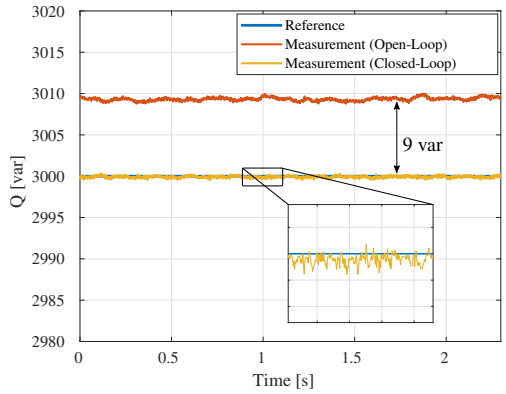

Fig. 15. Reactive power profile considering power structure composed of two interleaved dc/dc converters in parallel connection and power factor close to 0, considering both open and closed loop.

Considering the same power structure, Figure 15 shows the reactive power profile with PF close to zero. The error of the open-loop approach reduces to 9 var and this is in line with the analysis shown in Figure 4.c since the error variation, in this case, is less than the case of PF equal to 0.707. It is important to note that the closed-loop, leads to approximately zero steady-state error.

The second analysis considers the structure shown in Figure 2.b, with two cascaded interleaved dc/dc converters. The control structure shown in Figure 3.c, where both active and reactive power is in a closed-loop, is compared with the traditional scheme. Figure 16 shows the active power profile considering PF equal to 0.707 and reference equal to 3000 W. It can be noticed that open-loop approach presents an error between measurement and reference equal to 4.5 W, while for closed-loop approach, the error of measured active power and the reference is close to zero. Considering the same power structure, Figure 17 shows active power profile with PF equal to 1. The error of open-loop approach increased to 25.5 W. For this case, the phase error ($\Delta\theta$) in current control is 1.13 degrees and amplitude error (ΔI) is 0.06 pu. Through mathematical analysis presented in previous section, the expected reactive power error is 27.43 W. This represents an estimation error of 7.57% concerning the measurement value of 25.5 W.

These results show that the proposed scheme ensures very low steady-state error in the active and reactive power.

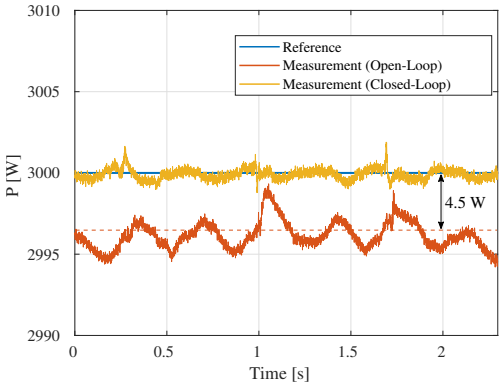

Fig. 16. Active power profile considering the power structure composed of two interleaved dc/dc converters in cascaded connection and power factor equal to 0.707, considering the active power in open and closed loop with reference equal to 3000 W.

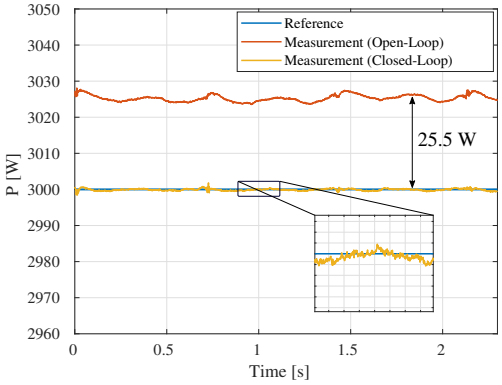

Fig. 17. Active power profile considering the power structure composed of two interleaved dc/dc converters in cascaded connection and power factor equal to 1, considering both open and closed loop.

VII. CONCLUSIONS

This paper approaches the active and reactive power control strategies applied to BESS. These strategies are applied in the inverter control along with the square dc-link voltage along with the stationary reference frame and instantaneous power theory. The experimental results, considering a deviation in the grid rated frequency, show that the steady-state error was reduced using the closed-loop for power components concerning the open-loop strategies addressed in the literature. Furthermore, it can be verified that the power component error depends on the power factor and the error of the current control loop. The control strategy proposed in this work is simple to be implemented and guarantees the reduction of the steady-state error in the power components. These errors can arise from several factors, such as discretization problems, bad control tunning, or grid frequency variation.

ACKNOWLEDGEMENTS

The authors would like to thank for the financial support by PD ANEEL/CEMIG D722, CNPq (Conselho Nacional de Desenvolvimento Científico e Tecnológico), Project 408059/2021-4, and FAPEMIG (Fundação de Amparo à Pesquisa do Estado de Minas Gerais), Project APQ-01187-18.

REFERENCES

[1] REN21, *Renewables 2020 Global Status Report*, Ph.D. thesis, Paris: REN21 Secretariat, Jun. 2020.

[2] H. Chen, T. N. Cong, W. Yang, C. Tan, Y. Li, Y. Ding, "Progress in electrical energy storage system: A critical review", *Progress in Natural Science*, vol. 19, no. 3, pp. 291–312, Mar. 2009.

[3] A. A. Akhil, G. Huff, A. B. Currier, B. C. Kaun, D. M. Rastler, S. B. Chen, A. L. Cotter, D. T. Bradshaw, W. D. Gauntlett, "DOE/EPRI 2013 Electricity Storage Handbook in Collaboration with NRECA", *Sandia Report*, vol. Sandia National Laboratories, Jul. 2013.

[4] D. I. Brandao, F. E. G. Mendes, R. V. Ferreira, S. M. Silva, I. A. Pires, "Active and Reactive Power Injection Strategies for Three-Phase Four-Wire Inverters During Symmetrical/Asymmetrical Voltage Sags", *IEEE Trans Ind Appl*, vol. 55, no. 3, Jan. 2019.

[5] M. I. M. Montero, E. R. Cadaval, F. B. Gonzalez, "Comparison of Control Strategies for Shunt Active Power Filters in Three-Phase Four-Wire Systems", *IEEE Trans Power Electron*, vol. 22, no. 1, pp. 229–236, Jan. 2007.

[6] Y. Yang, K. Zhou, F. Blaabjerg, "Enhancing the Frequency Adaptability of Periodic Current Controllers With a Fixed Sampling Rate for Grid-Connected Power Converters", *IEEE Trans Power Electron*, vol. 31, no. 10, pp. 7273–7285, Oct. 2016.

[7] A. Yazdani, R. Iravani, *Voltage-Sourced Converters in Power Systems: Modeling, Control, and Applications*, pp. 160–203, Jan. 2010.

[8] A. F. Cupertino, H. A. Pereira, "Chapter 21 - Next generation of grid-connected photovoltaic systems: modeling and control", *in* A. T. Azar, N. A. Kamal, eds., *Design, Analysis, and Applications of Renewable Energy Systems*, Advances in Nonlinear Dynamics and Chaos (ANDC), pp. 509–548, Academic Press, Jan. 2021.

[9] L. S. Xavier, A. F. Cupertino, H. A. Pereira, V. F. Mendes, "Partial Harmonic Current Compensation for Multifunctional Photovoltaic Inverters", *IEEE Trans Power Electron*, vol. 34, no. 12, pp. 11868–11879, Dec. 2019.

[10] N. Mukherjee, D. Strickland, "Control of Cascaded DC–DC Converter-Based Hybrid Battery Energy Storage Systems—Part I: Stability Issue", *IEEE Trans Ind Electron*, vol. 63, no. 4, pp. 2340–2349, Apr. 2016.

[11] W. Jiang, B. Fahimi, "Multiport Power Electronic Interface—Concept, Modeling, and Design", *IEEE Trans Power Electron*, vol. 26, no. 7, pp. 1890–1900, Jul. 2011.

[12] J. L. Da Silva, G. L. Dos Reis, S. I. Seleme, T. A. Meynard, "Control design and frequency analysis of an output filter in parallel interleaved converters", *in IEEE International Conference on Power and Energy (PECon)*, Jan. 2016.

[13] H.-C. Chen, C.-Y. Lu, U. S. Rout, "Decoupled Master-Slave Current Balancing Control for Three-Phase Interleaved Boost Converters", *IEEE Trans Power Electron*, vol. 33, no. 5, pp. 3683–3687, May 2018.

[14] S. Moayedi, V. Nasirian, F. L. Lewis, A. Davoudi, "Team-Oriented Load Sharing in Parallel DC–DC Converters", *IEEE Trans Ind Appl*, vol. 51, no. 1, pp. 479–490, Jan. 2015.

[15] G. Mondal, M. Neumeister, A. Hensler, S. Nielebock, "Modular parallel interleaved converter for high current application", *in IEEE 17th Workshop on Control and Modeling for Power Electronics (COMPEL)*, Jun. 2016.

[16] C. Jiang, H. Liu, "A Novel Interleaved Parallel Bidirectional Dual-Active-Bridge DC–DC Converter With Coupled Inductor for More-Electric Aircraft", *IEEE Trans Ind Electron*, vol. 68, no. 2, pp. 1759–1768, Feb. 2021.

[17] S. Vighetti, J.-P. Ferrieux, Y. Lembeye, "Optimization and Design of a Cascaded DC/DC Converter Devoted to Grid-Connected Photovoltaic Systems", *IEEE Trans Power Electron*, vol. 27, no. 4, pp. 2018–2027, Apr. 2012.

[18] C. Sun, M. Zhu, X. Zhang, J. Huang, X. Cai, "Output-Series Modular DC–DC Converter With Self-Voltage Balancing for Integrating Variable Energy Sources", *IEEE Trans Power Electron*, vol. 35, no. 11, pp. 11321–11327, Nov. 2020.

[19] A. I. Bratcu, I. Munteanu, S. Bacha, D. Picault, B. Raison, "Cascaded DC–DC Converter Photovoltaic Systems: Power Optimization Issues", *IEEE Trans Ind Electron*, vol. 58, no. 2, pp. 403–411, Feb. 2011.

[20] A. F. Cupertino, J. V. M. Farias, H. A. Pereira, S. I. Seleme, R. Teodorescu, "Comparison of DSCC and SDBC Modular Multilevel Converters for STATCOM Application During Negative Sequence Compensation", *IEEE Transactions on Industrial Electronics*, vol. 66, no. 3, pp. 2302–2312, Mar. 2019.

[21] A. F. Cupertino, L. S. Xavier, E. M. Brito, V. F. Mendes, H. A. Pereira, "Benchmarking of power control strategies for photovoltaic systems under unbalanced conditions", *International Journal of Electrical Power & Energy Systems*, vol. 106, pp. 335–345, Mar. 2019.

[22] L. S. Xavier, A. F. Cupertino, V. F. Mendes, H. A. Pereira, "Detection method for multi-harmonic current compensation applied in three-phase photovoltaic inverters", *in 12th IEEE International Conference on Industry Applications (INDUSCON)*, Nov. 2016.

[23] H. Akagi, Y. Kanazawa, A. Nabae, "Instantaneous Reactive Power Compensators Comprising Switching Devices without Energy Storage Components", *IEEE Trans Ind Appl*, vol. IA-20, no. 3, pp. 625–630, May 1984.

[24] Y. Yang, H. Wang, F. Blaabjerg, "Reactive Power Injection Strategies for Single-Phase Photovoltaic Systems Considering Grid Requirements", *IEEE Trans Ind Appl*, vol. 50, no. 6, pp. 4065–4076, Nov. 2014.

[25] V. Miñambres-Marcos, M. A. Guerrero-Martínez, E. Romero-Cadaval, P. González-Castrillo, "Grid-connected photovoltaic power plants for helping node voltage regulation", *IET Renewable Power Generation*, vol. 9, no. 3, pp. 236–244, Apr. 2015.

[26] P. Rodríguez, R. Teodorescu, I. Candela, A. V. Timbus, M. Liserre, F. Blaabjerg, "New positive-sequence voltage detector for grid synchronization of power converters under faulty grid conditions", *in 37th IEEE Power Electronics Specialists Conference*, Jun. 2006.

[27] R. Teodorescu, F. Blaabjerg, M. Liserre, P. C. Loh, "Proportional-resonant controllers and filters for grid-connected voltage-source converters", *IEE Proceedings - Electric Power Applications*, vol. 153, no. 5, pp. 750–762, Sep. 2006.

[28] A. G. Yepes, F. D. Freijedo, O. Lopez, J. Doval-Gandoy, "Analysis and Design of Resonant Current Controllers for Voltage-Source Converters by Means of Nyquist Diagrams and Sensitivity Function", *IEEE Transactions on Industrial Electronics*, vol. 58, no. 11, pp. 5231–5250, Nov. 2011.

[29] J. He, Y. W. Li, F. Blaabjerg, X. Wang, "Active Harmonic Filtering Using Current-Controlled, Grid-Connected DG Units With Closed-Loop Power Control", *IEEE Trans Power Electron*, vol. 29, no. 2, pp. 642–653, Apr. 2014.

[30] M. Parvez, M. F. M. Elias, N. A. Rahim, F. Blaabjerg, D. Abbott, S. F. Al-Sarawi, "Comparative Study of Discrete PI and PR Controls for Single-Phase UPS Inverter", *IEEE Access*, vol. 8, pp. 45584–45595, Jan. 2020.

[31] S. Golestan, E. Ebrahimzadeh, J. M. Guerrero, J. C. Vasquez, "An Adaptive Resonant Regulator for Single-Phase Grid-Tied VSCs", *IEEE Trans Power Electron*, vol. 33, no. 3, pp. 1867–1873, Mar. 2018.

[32] A. G. Yepes, F. D. Freijedo, J. Doval-Gandoy, O. López, J. Malvar, P. Fernandez-Comesaña, "Effects of Discretization Methods on the Performance of Resonant Controllers", *IEEE Trans Power Electron*, vol. 25, no. 7, pp. 1692–1712, Jul. 2010.

[33] J. He, B. Liang, Y. W. Li, C. Wang, "Simultaneous Microgrid Voltage and Current Harmonics Compensation Using Coordinated Control of Dual-Interfacing Converters", *IEEE Trans Power Electron*, vol. 32, no. 4, pp. 2647–2660, Apr. 2017.

BIOGRAPHIES

Lucas Santana Xavier, received the B.Sc. degree in electrical engineering from the Federal University of Viçosa, Viçosa, Brazil, and the M.Sc.degree in electrical engineering from the Federal University of Minas Gerais, Belo Horizonte, Brazil, in 2016 and 2018, respectively. He is currently working toward the Ph.D. degree in design and control of grid-connected converters for battery energy storage systems at the Federal University of Minas Gerais.

Allan Fagner Cupertino, Allan Fagner received the B.S. degree in electrical engineering from the Federal University of Viçosa (UFV) in 2013, the M.S. and Ph.D. degrees in Electrical Engineering from the Federal University of Minas Gerais (UFMG) in 2015 and 2019, respectively. He was a guest Ph.D. at the Department of Energy Technology, Aalborg University from 2018 to 2019. Since 2014, he has been with the Materials Engineering Department at the Federal Center of Technological Education of Minas Gerais (CEFET). His main research interests include renewable power generation systems, multifunctional inverters, modular multilevel converters, and reliability of power electronics-based systems. Prof. Cupertino was the recipient of the President Bernardes Silver Medal in 2013. He received the SOBRAEP Ph.D. Thesis Award in 2020 and the IEEE IAS CMD Student Thesis Contest in 2021.

Heverton Augusto Pereira, received the B.S. degree in electrical engineering from the Federal University of Viçosa (UFV), Viçosa, Brazil, the M.Sc. degree in electrical engineering from the University of Campinas, Campinas, Brazil, and the Ph.D. degree from the Federal University of Minas Gerais, Belo Horizonte, Brazil, in 2007, 2009, and 2015, respectively. In 2014, he was a Guest Ph.D. Scholar with the Department of Energy Technology, Aalborg University, Aalborg, Denmark. Since 2009, he has been an Adjunct Professor with the Electric Engineering Department, UFV. His main research interests include grid-connected converters for photovoltaic and wind power systems, and high-voltage dc/flexible ac transmission system based on MMC.

Victor Flores Mendes , received the B.E.E. degree incontrol and automation engineering, and the M.E.E.and Ph.D. degrees in electrical engineering fromthe Federal University of Minas Gerais (UFMG),Belo Horizonte, Brazil, in 2008, 2009, and 2013,respectively.During 2010, he developed a part of his thesiswith the Dresden University of Technology, Dresden,Germany. In 2020, he was a Postdoctoral Researcherwith Laboratoire Laplace, Toulouse, France. He iscurrently a Professor with UFMG, Belo Horizonte.His main research areas are wind and photovoltaic energy conversion, applications and control of power electronics, and power quality aspects of distributedgeneration grid integration.